

Searching for gluon quartic gauge couplings at muon colliders using the auto-encoder

Yu-Ting Zhang* and Xin-Tong Wang[†]

Department of Physics, Liaoning Normal University, Dalian 116029, China

Ji-Chong Yang[‡]

Department of Physics, Liaoning Normal University, Dalian 116029, China and

Center for Theoretical and Experimental High Energy Physics,

Liaoning Normal University, Dalian 116029, China

Abstract

One of the difficulties one has to face in the future phenomenological studies of the new physics (NP), is the need to deal with increasing amounts of data. It is therefore increasingly important to improve the efficiency in the phenomenological study of the NP. Whether it is the use of the Standard Model effective field theory (SMEFT), the use of machine learning (ML) algorithms, or the use of quantum computing, all are means of improving the efficiency. In this paper, we use a ML algorithm, the auto-encoder (AE), to study the dimension-8 operators in the SMEFT which contribute to the gluon quartic gauge couplings (gQGCs) at muon colliders. The AE is one of the ML algorithms that has the potential to be accelerated by the quantum computing. It is found that the AE-based anomaly detection algorithm can be used as event selection strategy to study the gQGCs at the muon colliders, and is effective compared with traditional event selection strategies.

I. INTRODUCTION

Supported by the large amount of experimental evidences, it can be concluded that the Standard Model (SM) is able to describe and explain the vast majority of phenomena in particle physics, with a few rare exceptions. These exceptions include experimental results such as the neutrino mass [1–3], the W boson mass problem [4, 5], the muon $g-2$ problem [6–8], and more [9]. Besides, the SM cannot describe dark matter, gravity, etc. As a result, the existence of the new physics (NP) beyond the SM has been widely believed, and the search of NP as well as precision measurements have been at the forefront of interest in the high energy physics (HEP) community [10].

Both the search for NP and precision measurements require dealing with a large number of events. With more and more data to be processed, more efficient ways to search for NP are called for. One of the reasons why the SM effective field theory (SMEFT) [11–14] has been widely used in the phenomenological study of NP in recent years is that SMEFT has an outstanding advantage of searching for NP signals with high efficiency. In the SMEFT, the NP particles are integrated out, and the NP effects become new interactions of known

* 976982345@qq.com

† 2226769965@qq.com

‡ yangjichong@lnmu.edu.cn; Corresponding author

particles. Formally, the new interactions appear as higher dimension operators with Wilson coefficients suppressed by powers of a NP scale Λ . The operators that are most likely to be found correspond to the operators with Wilson coefficients that are least suppressed by Λ . In stead of dealing with various NP models, the number of operators to be considered at a specific order of Λ in the SMEFT is finite. However, as the importance of the dimension-8 operators in the SMEFT has been realized [15–18], more and more phenomenological studies have been devoted to the dimension-8 operators in recent years [19–43]. For one generation of fermions, there are 895 baryon number conserving dimension-8 operators [44, 45], and there are even more operators if one considers operators with dimension more than eight. A procedure to select the events which does not rely on operators to be searched for can further improve efficiency.

Machine learning (ML) algorithms are one of the ways to process the data efficiently. ML is a multidisciplinary cross-discipline for studying how computers can mimic and implement human learning behaviors in order to acquire new knowledge, and has already been used in HEP studies [46–55]. ML algorithms have an advantage in processing complex data, and one of its common applications is anomaly detection (AD). When using AD to search for NP models, its implementation is often independent of the NP model to be searched. While hyperparameters in ML algorithms will often be NP model-dependent, the procedure of tuning of hyperparameters is usually common for different NP models. Based on this, an event selection strategy utilizing AD can be viewed as an automated event selection strategy. The use of AD algorithms in phenomenological studies is a hot topic in recent years [56–65].

Meanwhile, quantum computing is another effective way to deal with large amounts of data. Many ML algorithms can be implemented by quantum computing [66–68], an example of which is the auto-encoder (AE) algorithm [69, 70]. AE is an unsupervised learning dimensionality reduction algorithm using artificial neural networks (ANN), which is at the same time capable of AD. Therefore, it can be expected that AE can be used to detect NPs, and AE has already been used in phenomenological studies in HEP [63, 64, 71, 72]. Analogous to the principal component analysis (PCA) algorithm, the most common scenario for AE is data dimensionality reduction. While the PCA is a linear dimensionality reduction by solving the feature vector, the AE algorithm is a nonlinear dimensionality reduction. It is verified that, AD based on PCA is able to search for NP [62], therefore it can be expected that a similar approach works also for AE. Similar to PCA, AE has the potential for quantum

acceleration [73–76], and thus AE holds great promise for processing large amounts of data. To verify the feasibility of the AE algorithm in the search of high dimensional operators in the SMEFT, we use an AE algorithm based AD (AEAD) to study the gluon quartic gauge couplings (gQGCs) [77, 78] in this paper.

As an arena, the processes affected by gQGCs at muon colliders are considered. The muon colliders have been hotly discussed in recent years for searching for NP signals [79–89]. A muon collider has the advantage of being able to explore both high luminosity and high energy frontiers, while at the same time being less affected by the QCD background as a lepton collider. On the one hand, higher collision energies are better if one is committed to studying dimension-8 or even higher dimension operators, and on the other hand, higher luminosities require more efficient means of processing data. Thus, the processes at muon colliders that are affected by gQGCs are both worth studying and suitable for exploring the AEAD algorithm. For comparison with a conventional event selection strategy, in this paper the process $\mu^+\mu^- \rightarrow jj\nu\bar{\nu}$ is studied which has been studied in Ref. [90]. It has been shown that this process is sensitive to the gQGCs.

The rest of the paper is organized as follows, in section II, the dimension-8 operators contributing to the gQGCs are introduced. In section III, the event selection strategy based on AEAD algorithm is presented. In section IV, the numerical results and expected constraints on the operator coefficients are presented. Section V is a summary.

II. DIMENSION-8 OPERATORS CONTRIBUTING TO THE GQGCs

$M_0 \geq 1040$ GeV	$M_1 \geq 777$ GeV	$M_2 \geq 750$ GeV	$M_3 \geq 709$ GeV
$M_4 \geq 1399$ GeV	$M_5 \geq 1046$ GeV	$M_6 \geq 1010$ GeV	$M_7 \geq 954$ GeV

TABLE I: The constraints on the operator coefficients at 95% CL obtained by the process $gg \rightarrow \gamma\gamma$ at the LHC with $\sqrt{s} = 13$ TeV and $L = 36.7$ fb $^{-1}$ [77].

The gQGCs arise from the Born-Infeld (BI) extension of the SM, which was originally motivated by the idea that there should be an upper limit on the strength of the electromagnetic field [91]. It has been shown that, the BI model is also related to the M-theory inspired models [77, 78, 92–94]. In the SMEFT, the operators contributing to gQGCs appear

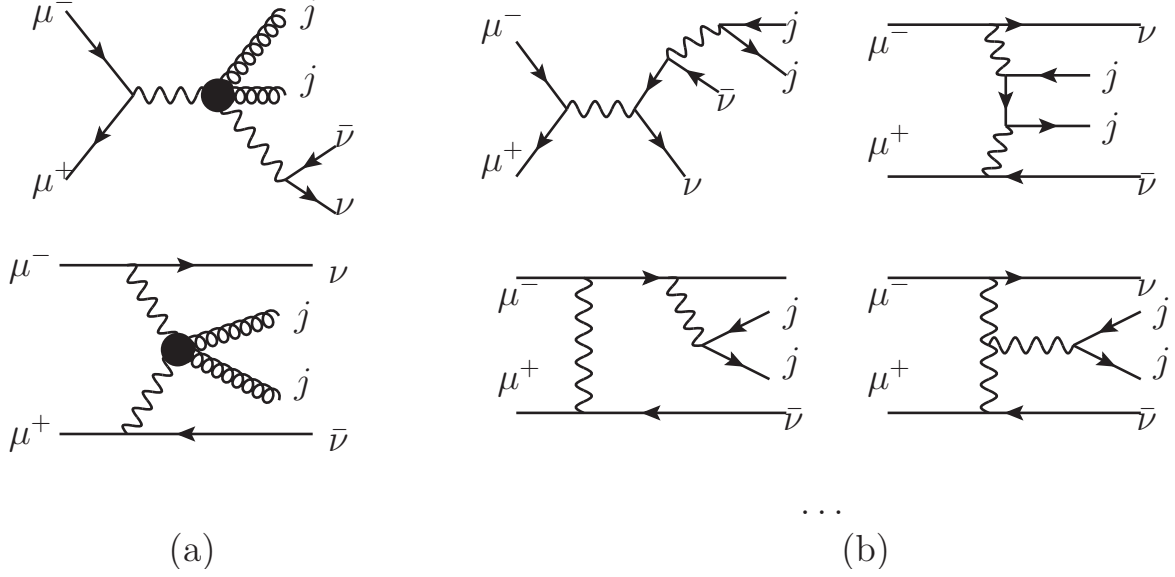


FIG. 1: Feynman diagrams for the process $\mu^+\mu^- \rightarrow jj\nu\bar{\nu}$, where (a) shows the Feynman diagrams of the gQGC contribution, and (b) shows the typical Feynman diagrams of the SM background.

at dimension-8,

$$\begin{aligned}
O_{gT,0} &= \frac{1}{16M_0^4} \sum_a G_{\mu\nu}^a G^{a,\mu\nu} \times \sum_i W_{\alpha\beta}^i W^{i,\alpha\beta}, \\
O_{gT,1} &= \frac{1}{16M_1^4} \sum_a G_{\alpha\nu}^a G^{a,\mu\beta} \times \sum_i W_{\mu\beta}^i W^{i,\alpha\nu}, \\
O_{gT,2} &= \frac{1}{16M_2^4} \sum_a G_{\alpha\mu}^a G^{a,\mu\beta} \times \sum_i W_{\nu\beta}^i W^{i,\alpha\nu}, \\
O_{gT,3} &= \frac{1}{16M_3^4} \sum_a G_{\alpha\mu}^a G_{\beta\nu}^a \times \sum_i W^{i,\mu\beta} W^{i,\nu\alpha}, \\
O_{gT,4} &= \frac{1}{16M_4^4} \sum_a G_{\mu\nu}^a G^{a,\mu\nu} \times B_{\alpha\beta} B^{\alpha\beta}, \\
O_{gT,5} &= \frac{1}{16M_5^4} \sum_a G_{\alpha\nu}^a G^{a,\mu\beta} \times B_{\mu\beta} B^{\alpha\nu}, \\
O_{gT,6} &= \frac{1}{16M_6^4} \sum_a G_{\alpha\mu}^a G^{a,\mu\beta} \times B_{\nu\beta} B^{\alpha\nu}, \\
O_{gT,7} &= \frac{1}{16M_7^4} \sum_a G_{\alpha\mu}^a G_{\beta\nu}^a \times B^{\mu\beta} B^{\nu\alpha},
\end{aligned} \tag{1}$$

where $G_{\mu\nu}^a$ is gluon field strengths, $W_{\mu\nu}^i$ and $B_{\mu\nu}$ denote electroweak field strengths, and M_i are mass scales associated with NP particles. For convenience, we define $f_i \equiv 1/(16M_i^4)$. The expected constraints on M_i at the Large Hadron Collider (LHC) with the center of

mass (c.m.) energy $\sqrt{s} = 13$ TeV, and luminosity $L = 36.7 \text{ fb}^{-1}$ obtained by using the process $gg \rightarrow \gamma\gamma$ are shown in Table I. The combined sensitivities of the $Z\gamma$ and $\gamma\gamma$ channels at the LHC with $\sqrt{s} = 13$ TeV and $L = 137 \text{ fb}^{-1}$ [78] are about three times of the ones shown in Table I.

The process $\mu^+\mu^- \rightarrow jj\nu\bar{\nu}$ at muon colliders can also be affected by the gQGCs [90]. Different from the case of a hadron collider that the operators are classified into four pairs with same Lorentz structures in phenomenological studies, at the muon colliders, the pairs can be decoupled. In particular, the process $\mu^+\mu^- \rightarrow jj\nu\bar{\nu}$ can be affected by the vector boson scattering (VBS) subprocess $W^+W^- \rightarrow gg$, which is associated with only $O_{gT,0,1,2,3}$ operators. The Feynman diagrams are shown in Fig. 1. Since the VBS contribution is logarithmically enhanced at large c.m. energies compared with the tri-boson process, we concentrate on the $O_{gT,0,1,2,3}$ operators. Taking $O_{gT,0}$ as an example, the 95% C.L. lower bounds on M_0 are about 27% of \sqrt{s} in the ‘optimistic’ cases, which shows a competitive sensitivity compared with the hadron colliders.

In the process $\mu^+\mu^- \rightarrow jj\nu\bar{\nu}$, there is no interference between the SM and gQGCs, which simplifies the procedure to obtain the expected constraints. However, there are two (anti-)neutrinos in the final state. This usually results in some loss of information, which in turn affects the efficiency of the event selection strategy. This just provides a place to test whether the AEAD algorithm is effective or not.

III. AUTO-ENCODER ANOMALY DETECTION

A. A brief introduction of the auto-encoder algorithm

AE is a type of ANN, which can be used in various applications, including data compression, feature extraction, denoising, data generation, etc. The structure of an AE is shown in Fig. 2, which is primarily composed of two parts, the encoder and the decoder. Both encoder and decoder can consist of multiple layers, with the neurons in the input layer denoted as x_i^{in} , and those in the output layer denoted as X_i^{out} . The data input to the input neurons and the data obtained from the output neurons are also notated as x_i^{in} and X_i^{out} , respectively, without leading to confusion. The goal to train an AE is to reconstruct the input data, i.e., the labels of the training data are just the input data, therefore the training

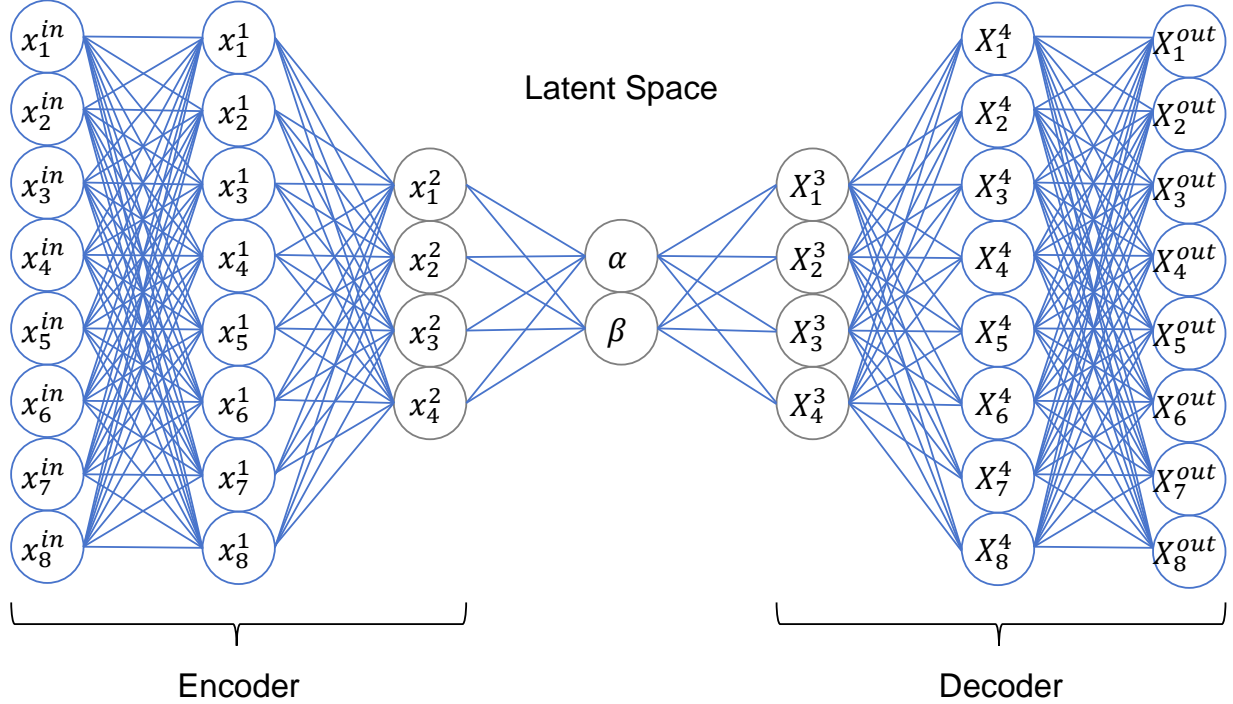


FIG. 2: The graphical representation of the AE. The AE network can be decomposed into two parts, where the encoder is consist of the $x^{in,1,2}$ and the latent layers, the decoder is consist of the latent, $X^{3,4,out}$ layers. In this paper, we use a dense connected network.

of an AE is unsupervised learning. The training objective is to minimize the reconstruction error between the x_i^{in} and X_i^{out} , aiming to obtain as similar a set of vectors from the output layer as possible after inputting a set of vectors into the input layer.

A well-trained AE can reproduce the input by utilizing two variables, α and β , along with the decoder network. Being able to reconstruct the input data indicates that, the information in α and β and in the decoder is enough to describe the data. Also, this means that the encoder is able to compress the information in the input data into two numbers, α and β (which is often called the latent space), i.e., data dimensionality reduction.

The reason an AE can achieve data dimensionality reduction lies in the fact that, the features of the input data are not independent. The encoder learns the relationships among the features and compresses them into α and β variables, which can then be used by the decoder to reconstruct the X_i^{out} . This mechanism of AE can be used for AD. At first, AE is trained on the SM events. Since the events are generated according to the physical laws of the SM, the relationships between the features learned by the AE are also related to the physical laws of the SM shaded behind them. At the same time, it can be expected

that the reconstruction of the events generated according to the physical laws of the NP will be less accurate than that of the SM, because the AE has not learned the relationships between the features of the events of the NP. The mean squared error (mse) defined as $d = \sum_i^N (x_i^{in} - X_i^{out}) / N$ can be used to represent the reconstruction error. In AEAD, d can also be used as an anomaly score. It can be expected that d is larger for the NP events compared with those of the SM events, therefore can be used to select the NP events.

B. The event selection strategy based on AEAD

Following the above idea, the AEAD event selection strategy can be summarized as follows,

- Generate the training and validation data sets using Monte Carlo (MC) simulation, which consist of the events from the SM.
- Train AE, and use the validation data set to avoid overfitting.
- For a test data set, which can be either obtained from the experiment or from MC simulation, calculate d for each event.
- Use a threshold d_{th} to select events, i.e. select the events with $d > d_{th}$, where d_{th} can be tuned according to the signal significance.

Note that, although the AE is unsupervised ML algorithm, in AEAD the SM data set is used in the training phase, therefore the AEAD is no longer unsupervised. However, the NP data sets are not used in the training phase. The test data set can be from the experiment, and there is no need to know whether it contains NP or what kind of NP it might contain. It can be expected that, the signal of NP can be traced by the AEAD whenever the test data set contains events that differ from the law of the SM.

IV. NUMERICAL RESULTS

A. Data preparation

To compare with the traditional event selection strategy, in this paper, we use the same events generated as in Ref. [90]. The events are generated using MC simulation with the

\sqrt{s} (TeV)	3	10	14	30
σ_{SM} (fb)	868.8	1454.8	1608.7	1898.8
$\hat{\sigma}_{\text{SM}}$ (fb)	722.9	1191.9	1315.5	1542.4
\tilde{f}_0 (TeV $^{-4}$)	1	0.012	0.004	0.00035
$\sigma_{gT,0}(\tilde{f}_0)$ (fb)	3.21	1.15	1.12	1.14
$\hat{\sigma}_{gT,0}(\tilde{f}_0)$ (fb)	3.21	1.15	1.12	1.14
\tilde{f}_1 (TeV $^{-4}$)	1.5	0.02	0.007	0.0006
$\sigma_{gT,1}(\tilde{f}_1)$ (fb)	3.55	1.38	1.44	1.34
$\hat{\sigma}_{gT,1}(\tilde{f}_1)$ (fb)	3.52	1.37	1.43	1.33
$\tilde{f}_{2,3}$ (TeV $^{-4}$)	3	0.03	0.012	0.0012
$\sigma_{gT,2}(\tilde{f}_2)$ (fb)	3.83	0.956	1.34	1.78
$\hat{\sigma}_{gT,2}(\tilde{f}_2)$ (fb)	3.82	0.955	1.34	1.78
$\sigma_{gT,3}(\tilde{f}_3)$ (fb)	4.12	0.924	1.27	1.61
$\hat{\sigma}_{gT,3}(\tilde{f}_3)$ (fb)	4.10	0.921	1.26	1.61

TABLE II: The cross-sections of the SM contribution and the NP contributions [90]. The NP contributions are cross-sections when the operator coefficients are \tilde{f}_i , \hat{f}_i used in the simulation are also shown. The cross-sections after N_j cut are denoted as $\hat{\sigma}$, which are also shown.

`MadGraph5_aMC@NLO` toolkit [95–97], where the standard cuts are set as the default. The parton shower is applied using `Pythia8` [98] with `NNPDF2.3` [99] as the parton distribution function. A fast detector simulation is performed using `Delphes` [100] with the muon collider card. The data cleaning and preparation phase is applied using `MLAnalysis` [101]. The ANN is constructed and trained using the `Keras` with the `TensorFlow` backend [102]. The events for the NP are generated with one operator at a time. The operator coefficients are set as the same as Ref. [90]. As an EFT, the SMEFT is only valid under a certain energy scale. One of the signals that the SMEFT is no longer valid is the violation of the unitarity [103–105], and the partial wave unitarity is often used in the phenomenological studies of the SMEFT to check whether the SMEFT is valid, which can sets bounds on the operator coefficients [106–112]. The operator coefficients used in the MC simulation are within the

constraints set by the partial wave unitarity bounds [90]. Denoting σ_{SM} as the cross-section of the SM contribution, and $\sigma_{gT,i}(\tilde{f}_i)$ as NP contributions with the operator coefficients to be \tilde{f}_i , respectively, the cross-sections and the listed in Table II.

After the events are generated, we require that the final states to have at least two jets. This requirement is denoted as the N_j cut, the cross-sections after N_j cut are denoted as $\hat{\sigma}_{\text{SM}}$ and $\hat{\sigma}_{gT,i}(\tilde{f}_i)$ which are also listed in Table II. Then an eight dimensional vector is made to represent each event such that $v = (p_t^{(1)}, p_x^{(1)}, p_y^{(1)}, p_z^{(1)}, p_t^{(2)}, p_x^{(2)}, p_y^{(2)}, p_z^{(2)})$, where $p^{(1)}$ and $p^{(2)}$ are the four momenta of hardest and second hardest jets. In the following, we consider only the 8-dimensional vectors described above, ignoring the physical meaning behind them.

\sqrt{s}	\bar{v}^1	\bar{v}^2	\bar{v}^3	\bar{v}^4	\bar{v}^5	\bar{v}^6	\bar{v}^7	\bar{v}^8
TeV	GeV	GeV	GeV	GeV	GeV	GeV	GeV	GeV
3	271.00	-0.14	-0.19	0.48	110.13	0.06	0.04	0.33
10	576.24	-0.01	0.14	3.00	225.00	-0.04	0.08	1.45
14	709.14	-0.21	-0.01	0.57	275.42	-0.02	-0.03	0.03
30	1053.94	0.15	0.01	4.64	398.96	-0.10	-0.13	1.74
\sqrt{s}	ϵ^1	ϵ^2	ϵ^3	ϵ^4	ϵ^5	ϵ^6	ϵ^7	ϵ^8
TeV	GeV	GeV	GeV	GeV	GeV	GeV	GeV	GeV
3	226.27	94.94	94.65	326.25	99.21	42.48	42.84	135.12
10	665.88	109.03	108.73	886.88	284.41	48.77	48.20	355.99
14	879.40	111.35	112.47	1118.43	371.30	50.10	52.11	456.52
30	1504.96	120.43	122.45	1829.17	603.26	56.48	56.66	718.74

TABLE III: The means \bar{v}^i and standard deviations ϵ^i of the components of the vectors \vec{v} over the training data sets.

For the SM contribution, we generate 1000000 events for each c.m. energy, taking the case of $\sqrt{s} = 3$ TeV as an example, 832056 events are left after the N_j cut, of which 400000 events consist the training data set, 100000 events consist the validation data set, and rest events consist the test data set. For each operator, 300000 events are generated, and all the events after the N_j cut are used as the test data set. The numbers of events after the N_j cut for the NP are generally more than 297000. Before the data sets are fed with the AE, a z-score standardization [113] is applied, i.e. the vectors \vec{v}_i are replaced by \vec{u}_i such

that $x_i^{in,j} = (v_i^j - \bar{v}^j) / \epsilon^j$, where $x_i^{in,j}, v_i^j$ are the j -th components of the \vec{x}_i^{in}, \vec{v} vectors, \bar{v}^j is the mean value of the j -th component over the training data set, and ϵ^j is the standard deviation of the j -th component over the training data set. \bar{v}^j and ϵ^j used in this paper are listed in Table III.

The AE is to reproduce the input vectors, therefore the labels of the training data sets are just as same as the input of the data sets.

B. Structure of the AE network

Since the events are represented by eight dimensional vectors, the number of neurons in the input layer of the encoder, and in the output layer of the decoder are both eight. The number of layers and the number of neurons in each layer is depicted in Fig. 2. In this paper, we use a densely connected ANN, taking the hidden layer x_i^1 as an example, values at neural x_i^1 can be calculated as $\vec{x}^1 = g^{in,1}(W^{in,1}\vec{x}^{in} + \vec{b}^{in})$, where $W^{i,j}$ is the weight matrix stored in the links between i -th and j -th layers, and \vec{b}^i is the basis vector stored in the neurons in i -th layer, and $g^{i,j}$ is the activation function between i -th and j -th layers. In this paper, we use the ‘‘LeakyReLU’’ function between the layers,

$$g(x) = \begin{cases} x, & x > 0, \\ \alpha x, & x \leq 0, \end{cases} \quad (2)$$

where $\alpha = 0.01$ is used in this paper. Specifically, $g^{in,1}, g^{1,2}, g^{latent,3}$, and $g^{3,4}$ are LeakyReLU functions, $g^{2,latent}$ and $g^{4,out}$ are linear activation functions. The loss function defines how well the input vectors can be reproduced by the AE. In this paper, we use the mse as the loss function.

C. Early stopping

Overfitting is a situation where the model performs well on the training set but relatively poorly on the test set. In that case, the model is weak in predicting unknown data. One of the methods to avoid overfitting is early stop.

The process of training the model is the process of updating the model parameters (i.e. $W^{i,j}$ and \vec{b}^i) through learning. In the training phase, the data set is divided into a training data set and a validation data set, and only the training data set is used to update the

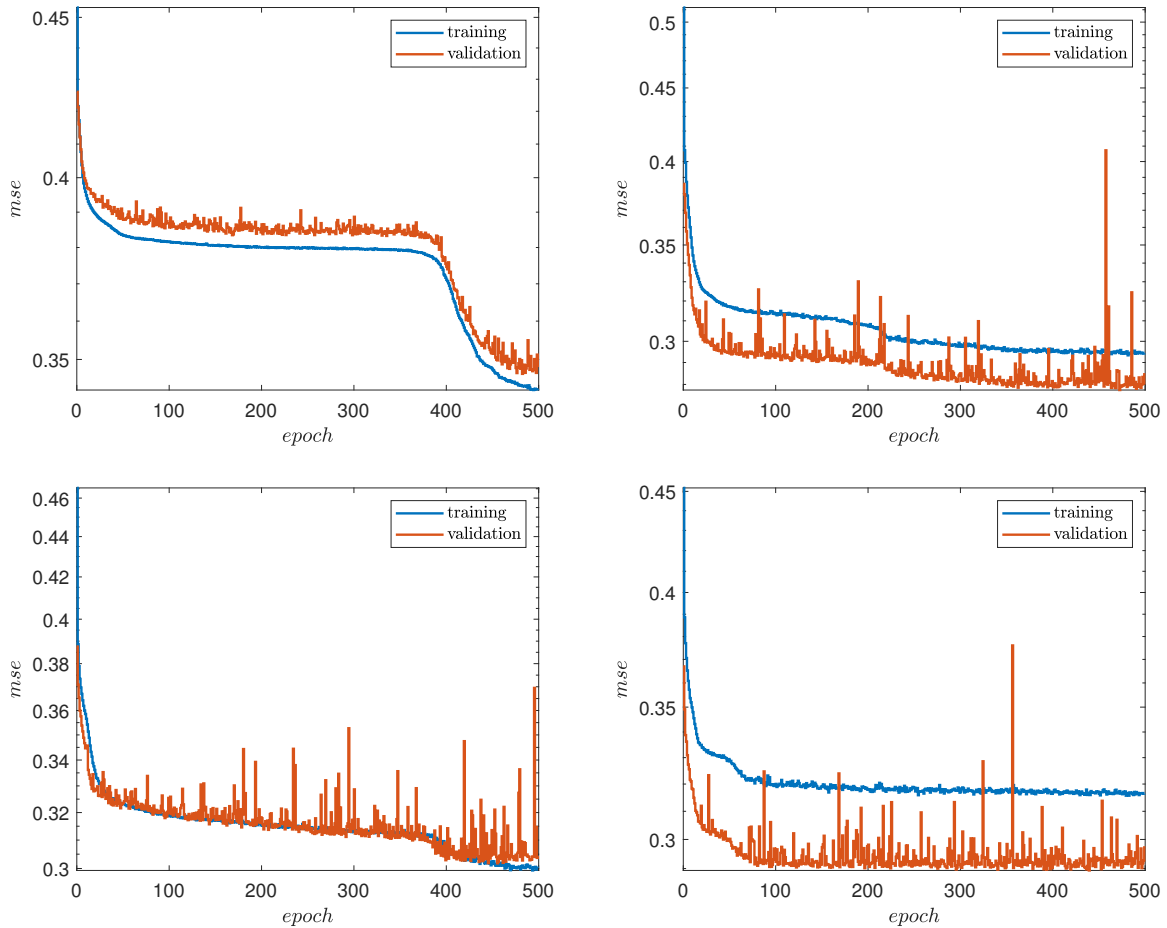


FIG. 3: The learning curves in the training phase. The top-left panel corresponds to $\sqrt{s} = 3$ TeV, the top-right panel corresponds to $\sqrt{s} = 10$ TeV, the bottom-left panel corresponds to $\sqrt{s} = 14$ TeV, and the bottom-right panel corresponds to $\sqrt{s} = 30$ TeV.

parameters. During the training process, the errors for the training set and validation set gradually decreases, and after reaching a critical point, the errors for the training set continue to decrease and the ones for the validation set start to increase. Early stopping is to prevent overfitting by stopping the training before the critical point, i.e., the number of iterations is truncated.

We use early stopping method to avoid overfitting in this paper. The mses for the training data set and the validation data set as functions of number of epochs are shown in Fig. 4. It can be seen that the mses of the validation sets stop to decrease when the numbers of epochs are about 500. In order to avoid overfitting, the numbers of epochs are chosen as above in this paper.

D. Distribution of the anomaly score

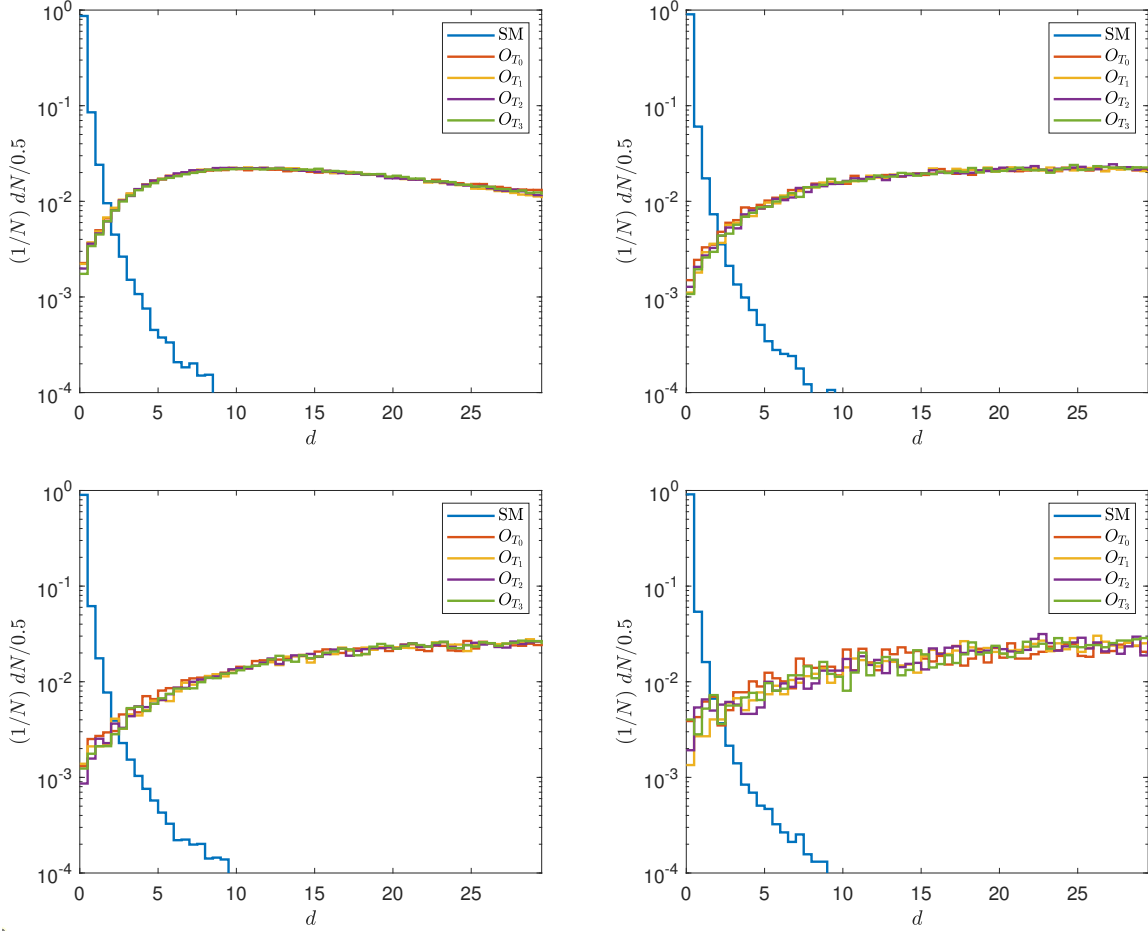


FIG. 4: The normalized distributions of d for the SM events and for the NP events in the test data sets. The top-left panel corresponds to $\sqrt{s} = 3$ TeV, the top-right panel corresponds to $\sqrt{s} = 10$ TeV, the bottom-left panel corresponds to $\sqrt{s} = 14$ TeV, and the bottom-right panel corresponds to $\sqrt{s} = 30$ TeV.

As described in the previous section, the AEAD uses how well the AE can reproduce the input as the anomaly score. That is, one can use d as the anomaly score. Note that d is defined using the data after z-score standardization, therefore is dimensionless.

In this subsection and in the following, we concentrate on the test data sets. The normalized distributions of d are shown in Fig. 4. It can be seen that the d for the SM background at different energies are generally small, thanks to the well trained AE. Meanwhile, the d for the NP signals are generally larger, and the larger the \sqrt{s} , the larger d . From the distri-

butions it can be concluded that d can provide a good discriminate ability to select the NP signals as expected.

E. Latent space distribution

It is known that AE can also be used as a data dimensionality reduction algorithm, a scheme that uses AE for classification uses AE as a data preparation stage. In combination with AE, other classification algorithms or AD algorithms can be applied in the latent space, i.e., the space consisting of the α and β values that are in the middle layer. Since the AE is trained to approximately reproduce events of the SM, this means that α and β contain the major information needed to reconstruct the events. That is, there are hidden relationships between the components of the vectors input to the AE, as a result, the components of the input vectors are not independent of each other. After dimension reduction, the events can be represented by a smaller number of variables, in our case, two variables α and β . Therefore, with the help of latent space, the features of the SM and the NP are more easily presented visually.

The distributions of the events in the latent spaces are shown in Fig. 5. It can be seen that, in the latent spaces, the NP events already distribute differently from the SM events. Due to the nonlinearity of the activation functions (segmented functions are used as the activation functions), different regions in the latent space often represent different functions that have been imposed to α and β in the decoder, and therefore represent different relationships among the components of the input/output vectors. The fact that the SM and NP events distributed differently in the latent space reflects the conjecture that, since the hidden relationships between the components are obtained by having the AE trained on the SM events, the events of the NP are not described by these relationships. This explains why d can be used to search for the NP signals.

F. Expected constraints on the operator coefficients

Usually, when the NP signals are not found, the task is to set constraints on the operator coefficients. This can be done by using the statistical signal significance which is defined

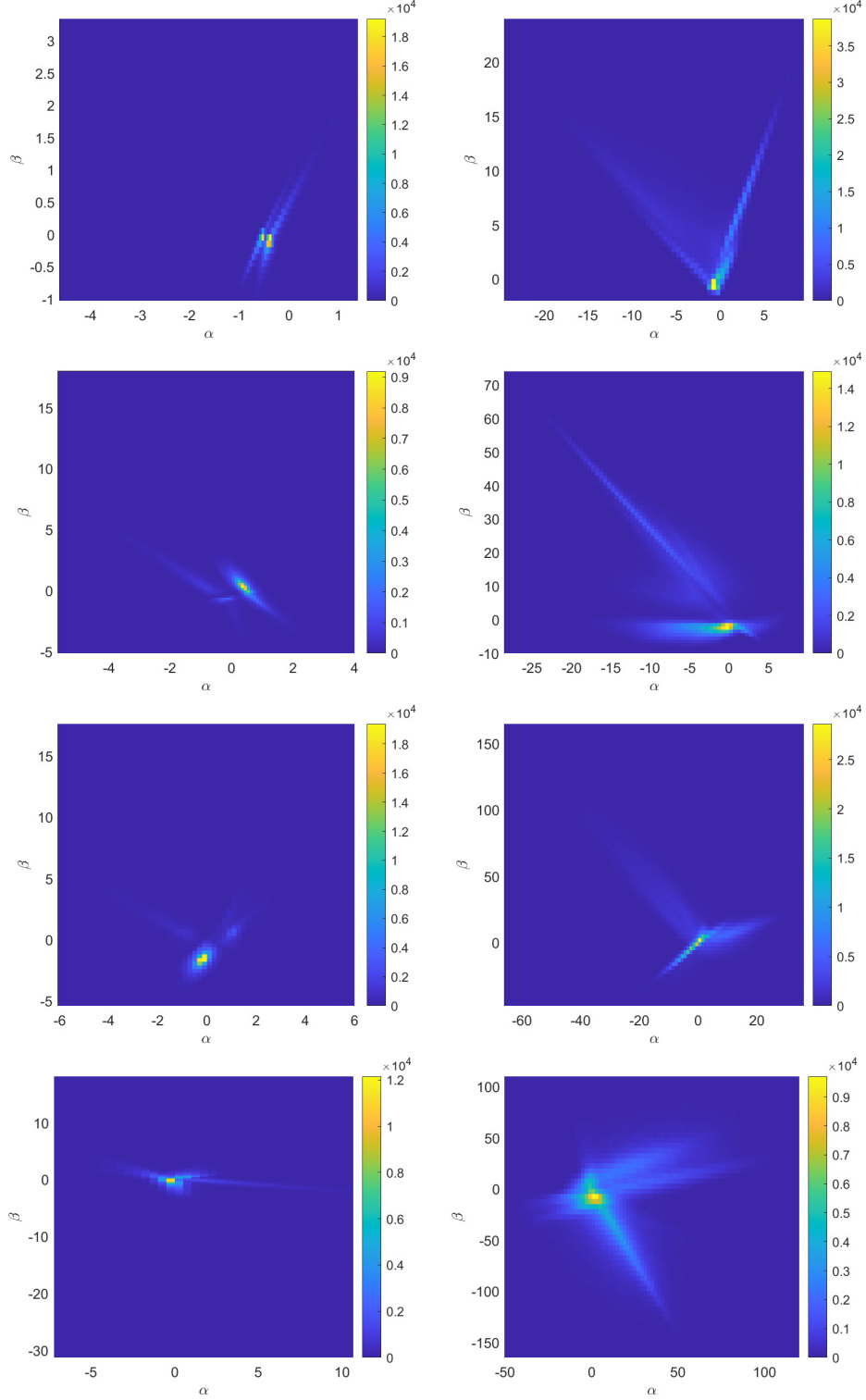


FIG. 5: The distributions of the test data set events in the latent space. The left panels are for the SM test data set, and the right panels are for the $O_{gT,0}$ test data sets. The first, second, third and the fourth rows correspond to $\sqrt{s} = 3$ TeV, 10 TeV, 14 TeV and 30 TeV, respectively.

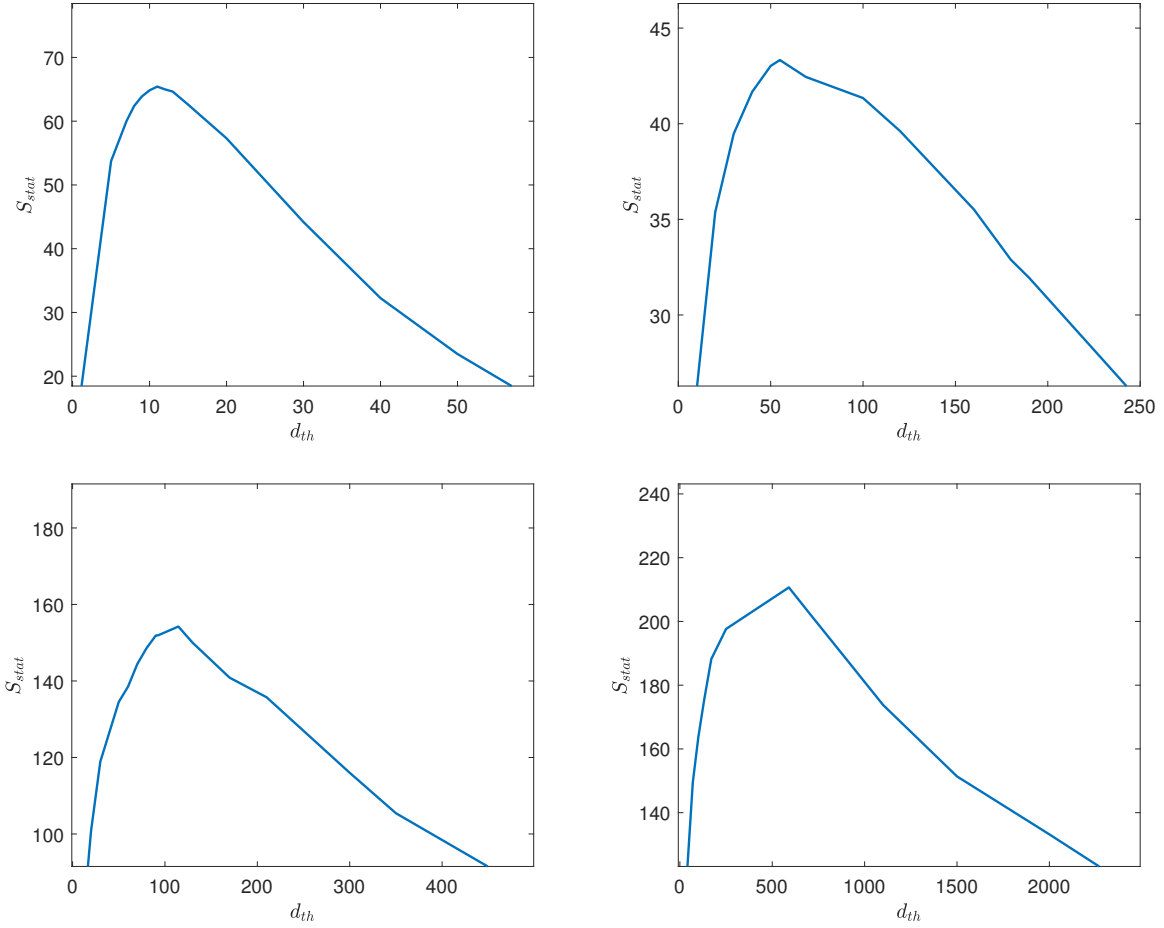


FIG. 6: The signal significances for the $O_{gT,0}$ at different energies as functions of d_{th} when $f_0 = \tilde{f}_0$ listed in Table II. The top-left panel corresponds to $\sqrt{s} = 3$ TeV, the top-right panel corresponds to $\sqrt{s} = 10$ TeV, the bottom-left panel corresponds to $\sqrt{s} = 14$ TeV, and the bottom-right panel corresponds to $\sqrt{s} = 30$ TeV.

as [114, 115],

$$\mathcal{S}_{\text{stat}} = \sqrt{2[(N_{\text{bg}} + N_s) \ln(1 + N_s/N_{\text{bg}}) - N_s]}, \quad (3)$$

where N_{bg} is the number of background events, N_s is the number of signal events. Since there is no interference between the SM and the NP contributions, the number of events after cuts can be obtained by $N_s = \varepsilon_{gT,i} L \times \sigma_{gT,i}$ and $N_{\text{bg}} = \varepsilon_{\text{SM}} L \times \sigma_{\text{SM}}$, where ε is the cut efficiency, σ is the cross-section, and L is the luminosity.

The luminosities in the “conservative” case for the muon colliders at $\sqrt{s} = 3$ TeV, 10 TeV, 14 TeV and 30 TeV are $L = 1 \text{ ab}^{-1}$, 10 ab^{-1} , 10 ab^{-1} and 10 ab^{-1} , respectively [86]. Taking

$f_i = \tilde{f}_i$ where \tilde{f}_i are listed in Table II, the $\mathcal{S}_{\text{stat}}$ as functions of d_{th} can be calculated, which are shown in Fig. 6. In the following, we choose d_{th} which maximizes the $\mathcal{S}_{\text{stat}}$ according to Fig. 6. At $\sqrt{s} = 3$ TeV, 10 TeV, 14 TeV and 30 TeV, we use $d_{th} > 11.0$, $d_{th} > 56.0$, $d_{th} > 114.5$ and $d_{th} > 584.3$, respectively.

The expected constraints on f_i and M_i in both the “conservative” and “optimistic” cases [86] are calculated, and listed in Tables IV and V. It can be seen that, the expected constraints derived by the AEAD are generally better than those derived using the traditional method. The expected constraints on f_i at 95% C.L. level ($S_{\text{stat}} = 2$) are compared with those from the traditional method [90] in Fig. 7. Except for the case of $O_{gT,2}$ at $\sqrt{s} = 14$ TeV, the AEAD performs better. It can be concluded that the AEAD can archive better results.

V. SUMMARY

With the potential for acceleration using quantum computing, the role of AE in searching for signals of NP becomes important, especially since NP has yet to show clear signs, and the search for NP cannot avoid dealing with increasing amounts of data for the foreseeable future. In this paper, the process of searching for NP signals using AEAD is proposed. The procedure is independent of the content of the NP to be searched since only the SM data set is used in the training phase.

As an example, the $\mu^+\mu^- \rightarrow \nu\bar{\nu}jj$ process at muon colliders is considered, which is sensitive to the dimension-8 operators contributing to gQGCs. The event selection strategy based on AEAD is studied, and the expected constraints on the operator coefficients are calculated. It can be shown that, the constraints are generally tighter than those obtained by using a traditional event selection strategy. Therefore, it can be concluded that the AEAD is effective in the phenomenological study of SMEFT. It is expected that the AE algorithm accelerated by quantum computers can be even more efficient in the future.

ACKNOWLEDGMENTS

This work was supported in part by the National Natural Science Foundation of China under Grants No. 12147214, and the Natural Science Foundation of the Liaoning Scientific

	\mathcal{S}_{stat}	3 TeV 1 ab ⁻¹	10 TeV 10 ab ⁻¹	14 TeV 10 ab ⁻¹	30 TeV 10 ab ⁻¹
$ f_0 $ (10 ⁻³ TeV ⁻⁴)	2	< 152	< 1.21	< 0.352	< 0.021
	3	< 187	< 1.49	< 0.432	< 0.027
	5	< 243	< 1.93	< 0.561	< 0.035
M_0 (TeV)	2	> 0.800	> 2.68	> 3.65	> 7.29
	3	> 0.760	> 2.55	> 3.47	> 6.92
	5	> 0.712	> 2.39	> 3.25	> 6.48
$ f_1 $ (10 ⁻³ TeV ⁻⁴)	2	< 222	< 1.84	< 0.544	< 0.037
	3	< 273	< 2.26	< 0.668	< 0.046
	5	< 354	< 2.93	< 0.867	< 0.060
M_1 (TeV)	2	> 0.728	> 2.41	> 3.27	> 6.40
	3	> 0.692	> 2.29	> 3.11	> 6.08
	5	> 0.648	> 2.15	> 2.91	> 5.69
$ f_2 $ (10 ⁻³ TeV ⁻⁴)	2	< 422	< 3.34	< 0.97	< 0.062
	3	< 518	< 4.10	< 1.19	< 0.076
	5	< 673	< 5.31	< 1.55	< 0.099
M_2 (TeV)	2	> 0.620	> 2.08	> 2.83	> 5.64
	3	> 0.589	> 1.98	> 2.69	> 5.35
	5	> 0.552	> 1.85	> 2.52	> 5.01
$ f_3 $ (10 ⁻³ TeV ⁻⁴)	2	< 407	< 3.38	< 0.98	< 0.066
	3	< 500	< 4.14	< 1.21	< 0.081
	5	< 649	< 5.37	< 1.57	< 0.106
M_3 (TeV)	2	> 0.626	> 2.07	> 2.82	> 5.55
	3	> 0.595	> 1.97	> 2.68	> 5.27
	5	> 0.557	> 1.85	> 2.51	> 4.93

TABLE IV: Expected constraints on f_i and M_i in the “conservative” case at muon colliders.

	\mathcal{S}_{stat}	14 TeV	30 TeV
		20 ab ⁻¹	90 ab ⁻¹
$ f_0 $ (10 ⁻⁴ TeV ⁻⁴)	2	< 3.09	< 0.148
	3	< 3.79	< 0.181
	5	< 4.91	< 0.234
M_0 (TeV)	2	> 3.77	> 8.07
	3	> 3.58	> 7.67
	5	> 3.36	> 7.19
$ f_1 $ (10 ⁻⁴ TeV ⁻⁴)	2	< 4.77	< 0.249
	3	< 5.85	< 0.305
	5	< 7.58	< 0.394
M_1 (TeV)	2	> 3.38	> 7.08
	3	> 3.22	> 6.73
	5	> 3.01	> 6.31
$ f_2 $ (10 ⁻⁴ TeV ⁻⁴)	2	< 8.50	< 0.413
	3	< 10.4	< 0.506
	5	< 13.5	< 0.655
M_2 (TeV)	2	> 2.93	> 6.24
	3	> 2.78	> 5.93
	5	> 2.61	> 5.56
$ f_3 $ (10 ⁻⁴ TeV ⁻⁴)	2	< 8.61	< 0.440
	3	< 10.6	< 0.539
	5	< 13.7	< 0.698
M_3 (TeV)	2	> 2.92	> 6.14
	3	> 2.77	> 5.83
	5	> 2.60	> 5.47

TABLE V: Same as Table IV but for the “optimistic” case.

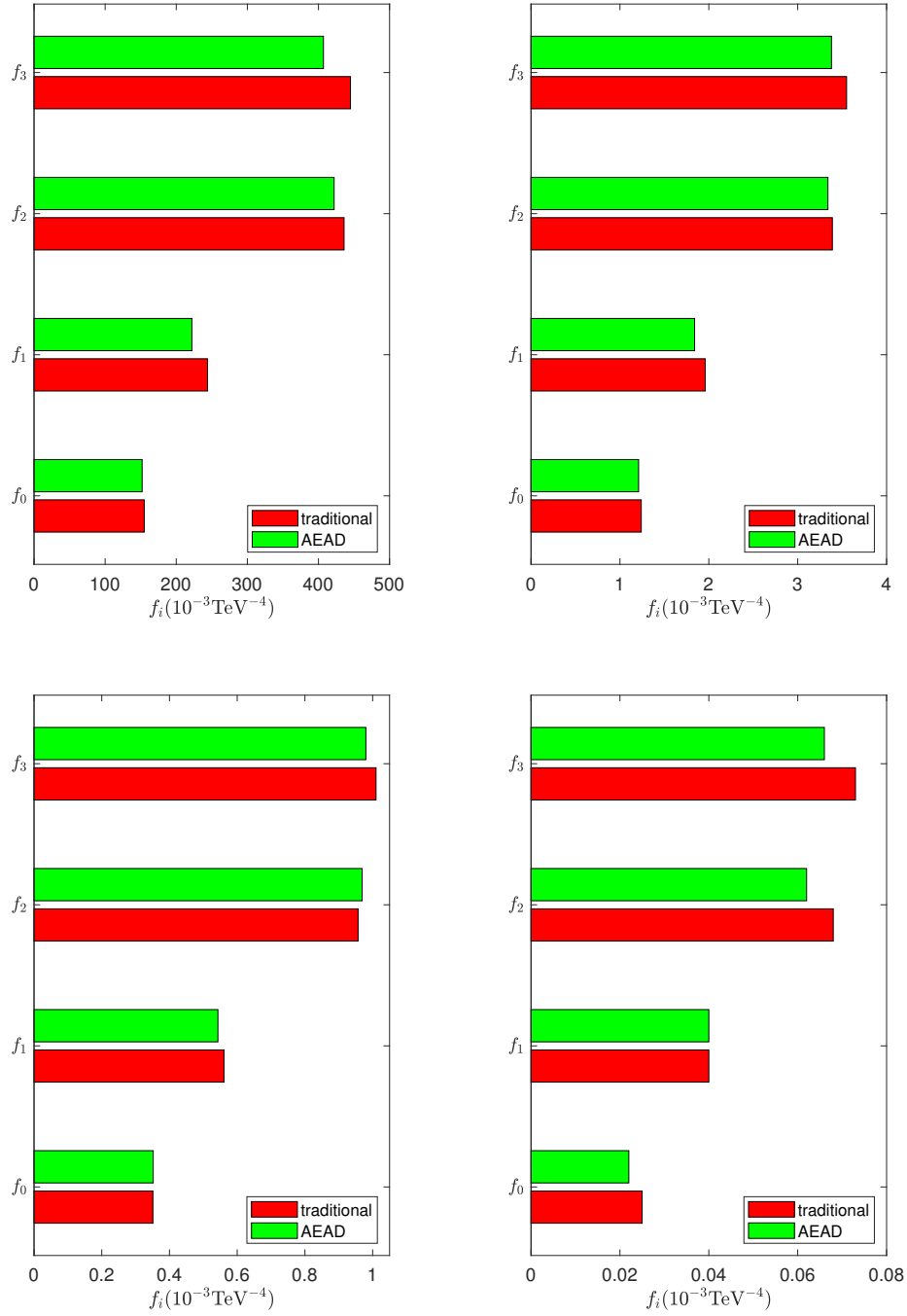


FIG. 7: The comparison of the expected constraints at 95% C.L. level obtained by a traditional event selection strategy [90], and the AEAD event selection strategy. The top-left panel corresponds to $\sqrt{s} = 3$ TeV, the top-right panel corresponds to 10 TeV, the bottom-left panel corresponds to 14 TeV, and the bottom-right panel corresponds to 30 TeV.

- [1] Y. Farzan and M. Tortola, Neutrino oscillations and Non-Standard Interactions, *Front. in Phys.* **6**, 10 (2018), arXiv:1710.09360 [hep-ph].
- [2] *Neutrino Non-Standard Interactions: A Status Report*, Vol. 2 (2019) arXiv:1907.00991 [hep-ph].
- [3] C. A. Argüelles *et al.*, Snowmass white paper: beyond the standard model effects on neutrino flavor: Submitted to the proceedings of the US community study on the future of particle physics (Snowmass 2021), *Eur. Phys. J. C* **83**, 15 (2023), arXiv:2203.10811 [hep-ph].
- [4] T. Aaltonen *et al.* (CDF), High-precision measurement of the W boson mass with the CDF II detector, *Science* **376**, 170 (2022).
- [5] J. de Blas, M. Pierini, L. Reina, and L. Silvestrini, Impact of the Recent Measurements of the Top-Quark and W-Boson Masses on Electroweak Precision Fits, *Phys. Rev. Lett.* **129**, 271801 (2022), arXiv:2204.04204 [hep-ph].
- [6] B. Abi *et al.* (Muon $g-2$), Measurement of the Positive Muon Anomalous Magnetic Moment to 0.46 ppm, *Phys. Rev. Lett.* **126**, 141801 (2021), arXiv:2104.03281 [hep-ex].
- [7] D. P. Aguillard *et al.* (Muon $g-2$), Measurement of the Positive Muon Anomalous Magnetic Moment to 0.20 ppm, *Phys. Rev. Lett.* **131**, 161802 (2023), arXiv:2308.06230 [hep-ex].
- [8] T. Aoyama *et al.*, The anomalous magnetic moment of the muon in the Standard Model, *Phys. Rept.* **887**, 1 (2020), arXiv:2006.04822 [hep-ph].
- [9] A. Crivellin and B. Mellado, Anomalies in Particle Physics, (2023), arXiv:2309.03870 [hep-ph].
- [10] J. Ellis, Outstanding questions: Physics beyond the Standard Model, *Phil. Trans. Roy. Soc. Lond. A* **370**, 818 (2012).
- [11] S. Weinberg, Baryon and Lepton Nonconserving Processes, *Phys. Rev. Lett.* **43**, 1566 (1979).
- [12] B. Grzadkowski, M. Iskrzynski, M. Misiak, and J. Rosiek, Dimension-Six Terms in the Standard Model Lagrangian, *JHEP* **10**, 085, arXiv:1008.4884 [hep-ph].
- [13] S. Willenbrock and C. Zhang, Effective Field Theory Beyond the Standard Model, *Ann. Rev. Nucl. Part. Sci.* **64**, 83 (2014), arXiv:1401.0470 [hep-ph].
- [14] E. Masso, An Effective Guide to Beyond the Standard Model Physics, *JHEP* **10**, 128,

- arXiv:1406.6376 [hep-ph].
- [15] D. R. Green, P. Meade, and M.-A. Pleier, Multiboson interactions at the LHC, *Rev. Mod. Phys.* **89**, 035008 (2017), arXiv:1610.07572 [hep-ex].
- [16] C. Zhang and S.-Y. Zhou, Convex Geometry Perspective on the (Standard Model) Effective Field Theory Space, *Phys. Rev. Lett.* **125**, 201601 (2020), arXiv:2005.03047 [hep-ph].
- [17] C. W. Murphy, Dimension-8 operators in the Standard Model Effective Field Theory, *JHEP* **10**, 174, arXiv:2005.00059 [hep-ph].
- [18] H.-L. Li, Z. Ren, J. Shu, M.-L. Xiao, J.-H. Yu, and Y.-H. Zheng, Complete set of dimension-eight operators in the standard model effective field theory, *Phys. Rev. D* **104**, 015026 (2021), arXiv:2005.00008 [hep-ph].
- [19] C. Zhang and S.-Y. Zhou, Positivity bounds on vector boson scattering at the LHC, *Phys. Rev. D* **100**, 095003 (2019), arXiv:1808.00010 [hep-ph].
- [20] Q. Bi, C. Zhang, and S.-Y. Zhou, Positivity constraints on aQGC: carving out the physical parameter space, *JHEP* **06**, 137, arXiv:1902.08977 [hep-ph].
- [21] M. Aaboud *et al.* (ATLAS), Studies of $Z\gamma$ production in association with a high-mass dijet system in pp collisions at $\sqrt{s} = 8$ TeV with the ATLAS detector, *JHEP* **07**, 107, arXiv:1705.01966 [hep-ex].
- [22] V. Khachatryan *et al.* (CMS), Measurement of the cross section for electroweak production of $Z\gamma$ in association with two jets and constraints on anomalous quartic gauge couplings in proton–proton collisions at $\sqrt{s} = 8$ TeV, *Phys. Lett. B* **770**, 380 (2017), arXiv:1702.03025 [hep-ex].
- [23] A. M. Sirunyan *et al.* (CMS), Measurement of the cross section for electroweak production of a Z boson, a photon and two jets in proton-proton collisions at $\sqrt{s} = 13$ TeV and constraints on anomalous quartic couplings, *JHEP* **06**, 076, arXiv:2002.09902 [hep-ex].
- [24] V. Khachatryan *et al.* (CMS), Measurement of electroweak-induced production of $W\gamma$ with two jets in pp collisions at $\sqrt{s} = 8$ TeV and constraints on anomalous quartic gauge couplings, *JHEP* **06**, 106, arXiv:1612.09256 [hep-ex].
- [25] A. M. Sirunyan *et al.* (CMS), Measurement of vector boson scattering and constraints on anomalous quartic couplings from events with four leptons and two jets in proton–proton collisions at $\sqrt{s} = 13$ TeV, *Phys. Lett. B* **774**, 682 (2017), arXiv:1708.02812 [hep-ex].
- [26] A. M. Sirunyan *et al.* (CMS), Measurement of differential cross sections for Z boson pair

- production in association with jets at $\sqrt{s} = 8$ and 13 TeV, Phys. Lett. B **789**, 19 (2019), arXiv:1806.11073 [hep-ex].
- [27] M. Aaboud *et al.* (ATLAS), Observation of electroweak $W^\pm Z$ boson pair production in association with two jets in pp collisions at $\sqrt{s} = 13$ TeV with the ATLAS detector, Phys. Lett. B **793**, 469 (2019), arXiv:1812.09740 [hep-ex].
- [28] A. M. Sirunyan *et al.* (CMS), Measurement of electroweak WZ boson production and search for new physics in WZ + two jets events in pp collisions at $\sqrt{s} = 13$ TeV, Phys. Lett. B **795**, 281 (2019), arXiv:1901.04060 [hep-ex].
- [29] V. Khachatryan *et al.* (CMS), Evidence for exclusive $\gamma\gamma \rightarrow W^+W^-$ production and constraints on anomalous quartic gauge couplings in pp collisions at $\sqrt{s} = 7$ and 8 TeV, JHEP **08**, 119, arXiv:1604.04464 [hep-ex].
- [30] A. M. Sirunyan *et al.* (CMS), Observation of electroweak production of same-sign W boson pairs in the two jet and two same-sign lepton final state in proton-proton collisions at $\sqrt{s} = 13$ TeV, Phys. Rev. Lett. **120**, 081801 (2018), arXiv:1709.05822 [hep-ex].
- [31] J. Ellis, H.-J. He, and R.-Q. Xiao, Probing Neutral Triple Gauge Couplings with $Z^*\gamma(\nu\bar{\nu}\gamma)$ Production at Hadron Colliders, (2023), arXiv:2308.16887 [hep-ph].
- [32] S. Spor, Probe of the anomalous neutral triple gauge couplings in photon-induced collision at future muon colliders, Nucl. Phys. B **991**, 116198 (2023), arXiv:2207.11585 [hep-ph].
- [33] S. Spor, E. Gurkanli, and M. Köksal, Search for the anomalous ZZ γ and Z $\gamma\gamma$ couplings via $\nu\nu\gamma$ production at the CLIC, Nucl. Phys. B **979**, 115785 (2022), arXiv:2203.02352 [hep-ph].
- [34] A. Yilmaz, Search for the limits on anomalous neutral triple gauge couplings via ZZ production in the $l\nu\nu$ channel at FCC-hh, Nucl. Phys. B **969**, 115471 (2021), arXiv:2102.01989 [hep-ph].
- [35] J. Ellis, H.-J. He, and R.-Q. Xiao, Probing new physics in dimension-8 neutral gauge couplings at e^+e^- colliders, Sci. China Phys. Mech. Astron. **64**, 221062 (2021), arXiv:2008.04298 [hep-ph].
- [36] A. Senol, H. Denizli, A. Yilmaz, I. Turk Cakir, and O. Cakir, Study on Anomalous Neutral Triple Gauge Boson Couplings from Dimension-eight Operators at the HL-LHC 10.5506/APhysPolB.50.1597 (2019), arXiv:1906.04589 [hep-ph].
- [37] A. Yilmaz, A. Senol, H. Denizli, I. Turk Cakir, and O. Cakir, Sensitivity on Anomalous Neutral Triple Gauge Couplings via ZZ Production at FCC-hh, Eur. Phys. J. C **80**, 173

- (2020), arXiv:1906.03911 [hep-ph].
- [38] J. Ellis, S.-F. Ge, H.-J. He, and R.-Q. Xiao, Probing the scale of new physics in the $ZZ\gamma$ coupling at e^+e^- colliders, *Chin. Phys. C* **44**, 063106 (2020), arXiv:1902.06631 [hep-ph].
- [39] Y.-C. Guo, Y.-Y. Wang, J.-C. Yang, and C.-X. Yue, Constraints on anomalous quartic gauge couplings via $W\gamma jj$ production at the LHC, *Chin. Phys. C* **44**, 123105 (2020), arXiv:2002.03326 [hep-ph].
- [40] Y.-C. Guo, Y.-Y. Wang, and J.-C. Yang, Constraints on anomalous quartic gauge couplings by $\gamma\gamma \rightarrow W^+W^-$ scattering, *Nucl. Phys. B* **961**, 115222 (2020), arXiv:1912.10686 [hep-ph].
- [41] J.-C. Yang, Y.-C. Guo, C.-X. Yue, and Q. Fu, Constraints on anomalous quartic gauge couplings via $Z\gamma jj$ production at the LHC, *Phys. Rev. D* **104**, 035015 (2021), arXiv:2107.01123 [hep-ph].
- [42] Q. Fu, J.-C. Yang, C.-X. Yue, and Y.-C. Guo, The study of neutral triple gauge couplings in the process $e^+e^- \rightarrow Z\gamma$ including unitarity bounds, *Nucl. Phys. B* **972**, 115543 (2021), arXiv:2102.03623 [hep-ph].
- [43] J.-C. Yang, Z.-B. Qing, X.-Y. Han, Y.-C. Guo, and T. Li, Tri-photon at muon collider: a new process to probe the anomalous quartic gauge couplings, *JHEP* **22**, 053, arXiv:2204.08195 [hep-ph].
- [44] C. F. Anders *et al.*, Vector boson scattering: Recent experimental and theory developments, *Rev. Phys.* **3**, 44 (2018), arXiv:1801.04203 [hep-ph].
- [45] B. Henning, X. Lu, T. Melia, and H. Murayama, 2, 84, 30, 993, 560, 15456, 11962, 261485, ...: Higher dimension operators in the SM EFT, *JHEP* **08**, 016, [Erratum: *JHEP* 09, 019 (2019)], arXiv:1512.03433 [hep-ph].
- [46] A. Radovic, M. Williams, D. Rousseau, M. Kagan, D. Bonacorsi, A. Himmel, A. Aurisano, K. Terao, and T. Wongjirad, Machine learning at the energy and intensity frontiers of particle physics, *Nature* **560**, 41 (2018).
- [47] P. Baldi, P. Sadowski, and D. Whiteson, Searching for Exotic Particles in High-Energy Physics with Deep Learning, *Nature Commun.* **5**, 4308 (2014), arXiv:1402.4735 [hep-ph].
- [48] J. Ren, L. Wu, J. M. Yang, and J. Zhao, Exploring supersymmetry with machine learning, *Nucl. Phys. B* **943**, 114613 (2019), arXiv:1708.06615 [hep-ph].
- [49] M. Abdughani, J. Ren, L. Wu, and J. M. Yang, Probing stop pair production at the LHC with graph neural networks, *JHEP* **08**, 055, arXiv:1807.09088 [hep-ph].

- [50] J. Ren, L. Wu, and J. M. Yang, Unveiling CP property of top-Higgs coupling with graph neural networks at the LHC, *Phys. Lett. B* **802**, 135198 (2020), arXiv:1901.05627 [hep-ph].
- [51] M. Letizia, G. Losapio, M. Rando, G. Grosso, A. Wulzer, M. Pierini, M. Zanetti, and L. Rosasco, Learning new physics efficiently with nonparametric methods, *Eur. Phys. J. C* **82**, 879 (2022), arXiv:2204.02317 [hep-ph].
- [52] R. T. D’Agnolo, G. Grosso, M. Pierini, A. Wulzer, and M. Zanetti, Learning multivariate new physics, *Eur. Phys. J. C* **81**, 89 (2021), arXiv:1912.12155 [hep-ph].
- [53] R. T. D’Agnolo and A. Wulzer, Learning New Physics from a Machine, *Phys. Rev. D* **99**, 015014 (2019), arXiv:1806.02350 [hep-ph].
- [54] J.-C. Yang, J.-H. Chen, and Y.-C. Guo, Extract the energy scale of anomalous $\gamma\gamma \rightarrow W^+W^-$ scattering in the vector boson scattering process using artificial neural networks, *JHEP* **09**, 085, arXiv:2107.13624 [hep-ph].
- [55] J.-C. Yang, X.-Y. Han, Z.-B. Qin, T. Li, and Y.-C. Guo, Measuring the anomalous quartic gauge couplings in the $W^+W^- \rightarrow W^+W^-$ process at muon collider using artificial neural networks, *JHEP* **09**, 074, arXiv:2204.10034 [hep-ph].
- [56] A. De Simone and T. Jacques, Guiding New Physics Searches with Unsupervised Learning, *Eur. Phys. J. C* **79**, 289 (2019), arXiv:1807.06038 [hep-ph].
- [57] M. A. Md Ali, N. Badrud’din, H. Abdullah, and F. Kemi, Alternate methods for anomaly detection in high-energy physics via semi-supervised learning, *Int. J. Mod. Phys. A* **35**, 2050131 (2020).
- [58] E. Fol, R. Tomás, J. Coello de Portugal, and G. Franchetti, Detection of faulty beam position monitors using unsupervised learning, *Phys. Rev. Accel. Beams* **23**, 102805 (2020).
- [59] G. Kasieczka *et al.*, The LHC Olympics 2020 a community challenge for anomaly detection in high energy physics, *Rept. Prog. Phys.* **84**, 124201 (2021), arXiv:2101.08320 [hep-ph].
- [60] Y.-C. Guo, L. Jiang, and J.-C. Yang, Detecting anomalous quartic gauge couplings using the isolation forest machine learning algorithm, *Phys. Rev. D* **104**, 035021 (2021), arXiv:2103.03151 [hep-ph].
- [61] J.-C. Yang, Y.-C. Guo, and L.-H. Cai, Using a nested anomaly detection machine learning algorithm to study the neutral triple gauge couplings at an e^+e^- collider, *Nucl. Phys. B* **977**, 115735 (2022), arXiv:2111.10543 [hep-ph].
- [62] Y.-F. Dong, Y.-C. Mao, and J.-C. Yang, Searching for anomalous quartic gauge couplings

- at muon colliders using principal component analysis, *Eur. Phys. J. C* **83**, 555 (2023), arXiv:2304.01505 [hep-ph].
- [63] M. Crispim Romão, N. F. Castro, and R. Pedro, Finding New Physics without learning about it: Anomaly Detection as a tool for Searches at Colliders, *Eur. Phys. J. C* **81**, 27 (2021), [Erratum: *Eur.Phys.J.C* 81, 1020 (2021)], arXiv:2006.05432 [hep-ph].
- [64] M. van Beekveld, S. Caron, L. Hendriks, P. Jackson, A. Leinweber, S. Otten, R. Patrick, R. Ruiz De Austri, M. Santoni, and M. White, Combining outlier analysis algorithms to identify new physics at the LHC, *JHEP* **09**, 024, arXiv:2010.07940 [hep-ph].
- [65] M. Kuusela, T. Vatanen, E. Malmi, T. Raiko, T. Aaltonen, and Y. Nagai, Semi-Supervised Anomaly Detection - Towards Model-Independent Searches of New Physics, *J. Phys. Conf. Ser.* **368**, 012032 (2012), arXiv:1112.3329 [physics.data-an].
- [66] J. Biamonte, P. Wittek, N. Pancotti, P. Rebentrost, N. Wiebe, and S. Lloyd, Quantum machine learning, *Nature* **549**, 195 (2017).
- [67] M. Schuld, I. Sinayskiy, and F. Petruccione, An introduction to quantum machine learning, *Contemporary Physics* **56**, 172 (2015).
- [68] D. P. García, J. Cruz-Benito, and F. J. García-Peñalvo, Systematic Literature Review: Quantum Machine Learning and its applications, (2022), arXiv:2201.04093 [quant-ph].
- [69] C.-Y. Liou, J.-C. Huang, and W.-C. Yang, Modeling word perception using the elman network, *Neurocomputing* **71**, 3150 (2008), advances in Neural Information Processing (ICONIP 2006) / Brazilian Symposium on Neural Networks (SBRN 2006).
- [70] C.-Y. Liou, W.-C. Cheng, J.-W. Liou, and D.-R. Liou, Autoencoder for words, *Neurocomputing* **139**, 84 (2014).
- [71] M. Farina, Y. Nakai, and D. Shih, Searching for New Physics with Deep Autoencoders, *Phys. Rev. D* **101**, 075021 (2020), arXiv:1808.08992 [hep-ph].
- [72] O. Cerri, T. Q. Nguyen, M. Pierini, M. Spiropulu, and J.-R. Vlimant, Variational Autoencoders for New Physics Mining at the Large Hadron Collider, *JHEP* **05**, 036, arXiv:1811.10276 [hep-ex].
- [73] J. Romero, J. P. Olson, and A. Aspuru-Guzik, Quantum autoencoders for efficient compression of quantum data, *Quantum Science and Technology* **2**, 045001 (2017), arXiv:1612.02806 [quant-ph].
- [74] C. Bravo-Prieto, Quantum autoencoders with enhanced data encoding, *Machine Learning:*

- Science and Technology **2**, 035028 (2021).
- [75] D. Bondarenko and P. Feldmann, Quantum autoencoders to denoise quantum data, *Phys. Rev. Lett.* **124**, 130502 (2020).
- [76] A. Khoshaman, W. Vinci, B. Denis, E. Andriyash, H. Sadeghi, and M. H. Amin, Quantum Variational Autoencoder., *Quantum Sci. Technol* **4**, 014001 (2019).
- [77] J. Ellis and S.-F. Ge, Constraining Gluonic Quartic Gauge Coupling Operators with $gg \rightarrow \gamma\gamma$, *Phys. Rev. Lett.* **121**, 041801 (2018), arXiv:1802.02416 [hep-ph].
- [78] J. Ellis, S.-F. Ge, and K. Ma, Hadron collider probes of the quartic couplings of gluons to the photon and Z boson, *JHEP* **04**, 123, arXiv:2112.06729 [hep-ph].
- [79] D. Buttazzo, D. Redigolo, F. Sala, and A. Tesi, Fusing Vectors into Scalars at High Energy Lepton Colliders, *JHEP* **11**, 144, arXiv:1807.04743 [hep-ph].
- [80] J. P. Delahaye, M. Diemoz, K. Long, B. Mansoulié, N. Pastrone, L. Rivkin, D. Schulte, A. Skrinsky, and A. Wulzer, Muon Colliders, (2019), arXiv:1901.06150 [physics.acc-ph].
- [81] M. Lu, A. M. Levin, C. Li, A. Agapitos, Q. Li, F. Meng, S. Qian, J. Xiao, and T. Yang, The physics case for an electron-muon collider, *Adv. High Energy Phys.* **2021**, 6693618 (2021), arXiv:2010.15144 [hep-ph].
- [82] R. Franceschini and M. Greco, Higgs and BSM Physics at the Future Muon Collider, *Symmetry* **13**, 851 (2021), arXiv:2104.05770 [hep-ph].
- [83] R. Palmer *et al.*, Muon collider design, *Nucl. Phys. B Proc. Suppl.* **51**, 61 (1996), arXiv:acc-phys/9604001.
- [84] S. D. Holmes and V. D. Shiltsev, Muon Collider, in *Outlook for the Future*, edited by C. Joshi, A. Caldwell, P. Muggli, S. D. Holmes, and V. D. Shiltsev (Springer-Verlag Berlin Heidelberg, Germany, 2013) pp. 816–822, arXiv:1202.3803 [physics.acc-ph].
- [85] A. Costantini, F. De Lillo, F. Maltoni, L. Mantani, O. Mattelaer, R. Ruiz, and X. Zhao, Vector boson fusion at multi-TeV muon colliders, *JHEP* **09**, 080, arXiv:2005.10289 [hep-ph].
- [86] H. Al Ali *et al.*, The muon Smasher’s guide, *Rept. Prog. Phys.* **85**, 084201 (2022), arXiv:2103.14043 [hep-ph].
- [87] T. Han, Y. Ma, and K. Xie, High energy leptonic collisions and electroweak parton distribution functions, *Phys. Rev. D* **103**, L031301 (2021), arXiv:2007.14300 [hep-ph].
- [88] T. Han, Y. Ma, and K. Xie, Quark and gluon contents of a lepton at high energies, *JHEP* **02**, 154, arXiv:2103.09844 [hep-ph].

- [89] C. Aime *et al.*, Muon Collider Physics Summary, (2022), arXiv:2203.07256 [hep-ph].
- [90] J.-C. Yang, Y.-C. Guo, and Y.-F. Dong, Study of the gluonic quartic gauge couplings at muon colliders, (2023), arXiv:2307.04207 [hep-ph].
- [91] M. Born and L. Infeld, Foundations of the new field theory, Proc. Roy. Soc. Lond. A **144**, 425 (1934).
- [92] E. S. Fradkin and A. A. Tseytlin, Nonlinear Electrodynamics from Quantized Strings, Phys. Lett. B **163**, 123 (1985).
- [93] A. A. Tseytlin, Born-Infeld action, supersymmetry and string theory, , 417 (1999), arXiv:hep-th/9908105.
- [94] C. Cheung, K. Kampf, J. Novotny, C.-H. Shen, J. Trnka, and C. Wen, Vector Effective Field Theories from Soft Limits, Phys. Rev. Lett. **120**, 261602 (2018), arXiv:1801.01496 [hep-th].
- [95] J. Alwall, R. Frederix, S. Frixione, V. Hirschi, F. Maltoni, O. Mattelaer, H. S. Shao, T. Stelzer, P. Torrielli, and M. Zaro, The automated computation of tree-level and next-to-leading order differential cross sections, and their matching to parton shower simulations, JHEP **07**, 079, arXiv:1405.0301 [hep-ph].
- [96] N. D. Christensen and C. Duhr, FeynRules - Feynman rules made easy, Comput. Phys. Commun. **180**, 1614 (2009), arXiv:0806.4194 [hep-ph].
- [97] C. Degrande, C. Duhr, B. Fuks, D. Grellscheid, O. Mattelaer, and T. Reiter, UFO - The Universal FeynRules Output, Comput. Phys. Commun. **183**, 1201 (2012), arXiv:1108.2040 [hep-ph].
- [98] T. Sjöstrand, S. Ask, J. R. Christiansen, R. Corke, N. Desai, P. Ilten, S. Mrenna, S. Prestel, C. O. Rasmussen, and P. Z. Skands, An introduction to PYTHIA 8.2, Comput. Phys. Commun. **191**, 159 (2015), arXiv:1410.3012 [hep-ph].
- [99] R. D. Ball, V. Bertone, S. Carrazza, L. Del Debbio, S. Forte, A. Guffanti, N. P. Hartland, and J. Rojo (NNPDF), Parton distributions with QED corrections, Nucl. Phys. B **877**, 290 (2013), arXiv:1308.0598 [hep-ph].
- [100] J. de Favereau, C. Delaere, P. Demin, A. Giammanco, V. Lemaitre, A. Mertens, and M. Selvaggi (DELPHES 3), DELPHES 3, A modular framework for fast simulation of a generic collider experiment, JHEP **02**, 057, arXiv:1307.6346 [hep-ex].
- [101] Y.-C. Guo, F. Feng, A. Di, S.-Q. Lu, and J.-C. Yang, MLAnalysis: An open-source program for high energy physics analyses, Comput. Phys. Commun. **294**, 108957 (2024),

- arXiv:2305.00964 [hep-ph].
- [102] M. Abadi *et al.*, TensorFlow: Large-Scale Machine Learning on Heterogeneous Distributed Systems, (2016), arXiv:1603.04467 [cs.DC].
- [103] T. D. Lee and C.-N. Yang, THEORETICAL DISCUSSIONS ON POSSIBLE HIGH-ENERGY NEUTRINO EXPERIMENTS, Phys. Rev. Lett. **4**, 307 (1960).
- [104] M. Froissart, Asymptotic behavior and subtractions in the Mandelstam representation, Phys. Rev. **123**, 1053 (1961).
- [105] G. Passarino, W W scattering and perturbative unitarity, Nucl. Phys. B **343**, 31 (1990).
- [106] T. Corbett, O. J. P. Éboli, and M. C. Gonzalez-Garcia, Unitarity Constraints on Dimension-Six Operators, Phys. Rev. D **91**, 035014 (2015), arXiv:1411.5026 [hep-ph].
- [107] J. Layssac, F. M. Renard, and G. J. Gounaris, Unitarity constraints for transverse gauge bosons at LEP and supercolliders, Phys. Lett. B **332**, 146 (1994), arXiv:hep-ph/9311370.
- [108] T. Corbett, O. J. P. Éboli, and M. C. Gonzalez-Garcia, Unitarity Constraints on Dimension-six Operators II: Including Fermionic Operators, Phys. Rev. D **96**, 035006 (2017), arXiv:1705.09294 [hep-ph].
- [109] R. Gomez-Ambrosio, Vector Boson Scattering Studies in CMS: The $pp \rightarrow ZZjj$ Channel, Acta Phys. Polon. Supp. **11**, 239 (2018), arXiv:1807.09634 [hep-ph].
- [110] G. Perez, M. Sekulla, and D. Zeppenfeld, Anomalous quartic gauge couplings and unitarization for the vector boson scattering process $pp \rightarrow W^+W^+jjX \rightarrow \ell^+\nu_\ell\ell^+\nu_\ell jjX$, Eur. Phys. J. C **78**, 759 (2018), arXiv:1807.02707 [hep-ph].
- [111] E. d. S. Almeida, O. J. P. Éboli, and M. C. Gonzalez-Garcia, Unitarity constraints on anomalous quartic couplings, Phys. Rev. D **101**, 113003 (2020), arXiv:2004.05174 [hep-ph].
- [112] W. Kilian, S. Sun, Q.-S. Yan, X. Zhao, and Z. Zhao, Multi-Higgs boson production and unitarity in vector-boson fusion at future hadron colliders, Phys. Rev. D **101**, 076012 (2020), arXiv:1808.05534 [hep-ph].
- [113] D. Donoho and J. Jin, Higher criticism for detecting sparse heterogeneous mixtures, The Annals of Statistics **32**, 10.1214/009053604000000265 (2004).
- [114] G. Cowan, K. Cranmer, E. Gross, and O. Vitells, Asymptotic formulae for likelihood-based tests of new physics, Eur. Phys. J. C **71**, 1554 (2011), [Erratum: Eur.Phys.J.C 73, 2501 (2013)], arXiv:1007.1727 [physics.data-an].
- [115] P. A. Zyla *et al.* (Particle Data Group), Review of Particle Physics, PTEP **2020**, 083C01

(2020).